



HAL
open science

Toward the Control of the Smoldering Front in the Reaction-Trailing Mode in Oil Shale Semicoke Porous Media

Mohamed Sennoune, Sylvain Salvador, Michel Quintard

► To cite this version:

Mohamed Sennoune, Sylvain Salvador, Michel Quintard. Toward the Control of the Smoldering Front in the Reaction-Trailing Mode in Oil Shale Semicoke Porous Media. *Energy & Fuels*, 2012, vol. 26 (n° 6), pp. 3357-3367. <10.1021/ef300479d>. <hal-01688258>

HAL Id: hal-01688258

<https://hal.science/hal-01688258v1>

Submitted on 19 Jan 2018

HAL is a multi-disciplinary open access archive for the deposit and dissemination of scientific research documents, whether they are published or not. The documents may come from teaching and research institutions in France or abroad, or from public or private research centers.

L'archive ouverte pluridisciplinaire HAL, est destinée au dépôt et à la diffusion de documents scientifiques de niveau recherche, publiés ou non, émanant des établissements d'enseignement et de recherche français ou étrangers, des laboratoires publics ou privés.



HAL Authorization



Open Archive TOULOUSE Archive Ouverte (OATAO)
OATAO is an open access repository that collects the work of Toulouse researchers and makes it freely available over the web where possible.

This is an author-deposited version published in : <http://oatao.univ-toulouse.fr/>
Eprints ID : 8798

To link to this article : DOI:10.1021/ef300479d
URL : <http://dx.doi.org/10.1021/ef300479d>

To cite this version :
Sennoune, Mohamed and Salvador, Sylvain and Quintard, Michel
Toward the Control of the Smoldering Front in the Reaction-Trailing Mode in Oil Shale Semicoke Porous Media. (2012)
Energy & Fuels, vol. 26 (n° 6). pp. 3357-3367. ISSN 0887-0624

Any correspondence concerning this service should be sent to the repository administrator: staff-oatao@listes.diff.inp-toulouse.fr

Toward the Control of the Smoldering Front in the Reaction-Trailing Mode in Oil Shale Semicoke Porous Media

M. Sennoune,^{*,†} S. Salvador,[†] and M. Quintard[‡]

[†]Université de Toulouse, Mines Albi, CNRS, Centre de RAPSODEE, Campus Jarlard, F-81013 Albi CT cedex 09, France

[‡]Université de Toulouse, CNRS, IMFT, Allée Camille Soula F-31400, Toulouse, France

ABSTRACT: Results of an experimental investigation on the feasibility of propagating a smoldering front in reaction-trailing mode throughout an oil shale semicoke porous medium are reported. For oil recovery applications, this mode is particularly interesting to avoid low-temperature oxidation reactions, which appear simultaneously with organic matter devolatilization in the reaction-leading mode and are responsible for oxidation of part of the heavy oil. The particularity of this mode is that, contrary to the reaction-leading mode largely studied in the literature, the heat-transfer layer precedes the combustion layer. This leads to two separated high-temperature zones: (i) a devolatilization zone (free of oxygen), where the organic matter is thermally decomposed to incondensable gases, heavy oil, and fixed carbon, also called coke in the literature, without any oxidation, followed by (ii) an oxidation zone, where the fixed carbon left by devolatilization is oxidized. The transition from reaction-leading to reaction-trailing mode was obtained using low oxygen contents in the fed air. It is shown that two distinct layers, the heat-transfer layer and the combustion layer, propagate in a stable and repeatable way. The decrease of the oxygen fraction leads to a decrease of the smoldering temperature and to strongly limit the decarbonation of the mineral matrix. The CO₂ emissions are limited. Regardless of the front temperature, all of the fed oxygen is consumed and all of the fixed carbon is oxidized at the passage of the smoldering front.

1. INTRODUCTION

Smoldering combustion is a process of importance to a variety of applications, ranging from the recovery of oil from oil reservoirs (*in situ* combustion) to the processing of materials, such as coal, coke, wood, tar sand, oil shale, and waste products of industrial and agricultural operations. It is a combustion mode distinctly different from flaming. Indeed, it is characterized by a dominance of heterogeneous oxidation reactions occurring on the solid surface of the fuel or porous matrix.¹ In its most simplified form, it involves the combustion of a solid fuel, through the injection of an oxidizer agent.

When ignition occurs at the gas inlet, the smoldering front propagates in the direction of the injected gas, and the process is referred to as forward smoldering combustion. When ignition occurs at the opposite side, the reaction front propagates in the direction opposite of the gas flow and a process of a backward smoldering combustion develops. This paper is concerned by forward smoldering combustion.

During the forward smoldering combustion process, there are in reality two combustion layers propagating with constant, although not the same, velocities and separated by a region of constant high temperature called plateau. In the combustion layer, also called chemical front, fixed carbon (FC) oxidation occurs, while in the heat-transfer layer, also called thermal front, temperature changes are due to heat transfer between solid and gas. Two structures are possible, depending upon which layer has the greatest speed and, therefore, which layer precedes the other. The classical structure generally encountered in natural and industrial applications involving air and media with small carbon content is called reaction-leading (RL) mode. The velocity of the combustion layer is the greatest of the two velocities; therefore, the combustion layer precedes the heat-

transfer layer. The second structure, which is referred to as an inverted structure in the combustion literature,² is called the reaction-trailing (RT) mode. The velocity of the combustion layer is the smaller of the two layers, so that the heat-transfer layer precedes the combustion layer. The two situations are illustrated in Figure 1. The RT mode is not encountered in classical applications. Only theoretical description was given in the literature.^{2,3} Its feasibility under controlled conditions was not demonstrated, and this was the main motivation for this work.

The transition from the RL mode (classical mode) to the RT mode is theoretically possible and solely depends upon the value of a parameter δ ,³ which can be expressed as follows according to⁴

$$\delta = \frac{C_{p_g} c_{FC}^{in} - c_{FC}^{out}}{C_{p_s} c_O^{in} - c_O^{out}} \quad (1)$$

where C_{p_g} and C_{p_s} are the specific heats of the gas and solid, respectively, c_{FC}^{in} and c_{FC}^{out} are the initial and final fractions of the solid fuel (FC), and c_O^{in} and c_O^{out} are the initial and final fractions of the gaseous oxidizer (O₂).

The RL mode occurs if $\delta < 1$, and the RT mode occurs if $\delta > 1$. The case $\delta = 1$ separates the two structures and corresponds to a combustion temperature that is infinite in the approximate model used to derive eq 1.

The RT mode can be reached via two approaches: the increase of the amount of FC in the porous medium (which is

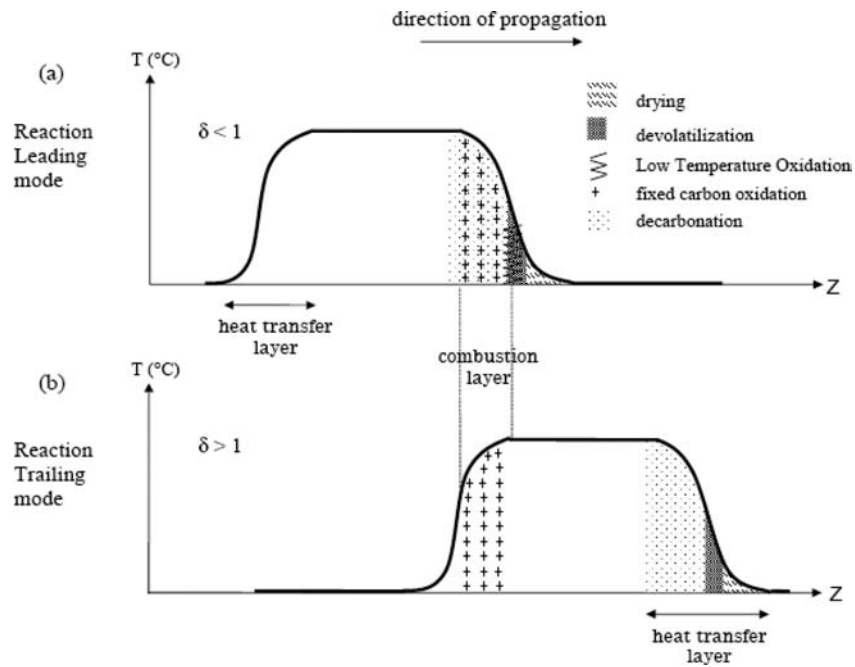


Figure 1. Probable localization of the different reaction zones in the (a) leading and (b) trailing modes.

not a controllable parameter in the case of *in situ* applications) or the decrease of the fraction of oxygen in the fed gas. The last approach will be adopted in the experimental work presented in this paper.

Before proceeding to the description of the experimental results, we present a brief description, on the basis of a literature review, of the RL and RT modes and discuss the potential advantages and drawbacks of the RT mode in oil shale applications, which represent a very industrial challenge for the next few decades.

1.1. RL Mode. As mentioned briefly in the previous paragraph, the most encountered structure of smoldering propagation is the RL mode. Many authors have examined this mode of propagation in different disciplines and for several materials.^{5–12} Smoldering in oil shale has also interested several authors. Oil shale is a sedimentary rock that contains a solid organic material embedded in a matrix of fine inorganic minerals and must be decomposed thermally in classical recovery processes. More recently, with regard to our study, Martins et al.¹³ established into details the structure of a smoldering front propagating in oil shale porous media. Later, Sennoune et al.¹⁴ proposed a new approach to reduce the CO₂ emissions resulting from the decarbonation of the mineral matrix at the passage of a smoldering front. It consists of varying the composition of the medium in FC and carbonates.

1.2. RT Mode. Only very few works are available in which the RT mode has been studied.

With regard to the experimental side, to our knowledge, the only carried out works are those presented by Voice and Wild¹⁵ for material sintering of applications, where the transition from the RL to the RT mode was obtained by varying the ambient oxygen. They reported that, with 35% of oxygen in the sintering atmosphere, the combustion layer becomes ahead of the heat-transfer layer (RT), so that a relatively low bed temperature is reached. As the proportion of oxygen is decreased, the two layers come closer until, at 9% of oxygen, the highest temperature is obtained. With only 4% of oxygen in the atmosphere, the heat-transfer layer becomes ahead of the

combustion layer and the RL mode is reached, giving a very slow rise in bed temperature and a low peak value.

With regard to the theoretical side, there has been only very limited investigations on the properties of this mode. Schult et al.² reported in their pioneering work that the structure of the RT wave consists of a high-temperature region with a leading heat-transfer layer and a trailing combustion layer, in which the oxygen is consumed and heat is released. The peak temperature of the smoldering front is affected by the oxygen fraction and not the gas flux.

According to Lempert et al.,¹⁶ the heat released by combustion is removed by the gas flow in the case of the RT mode, while in the case of the RL mode, it is removed through transport in the solid material. These two heat flows determine the type of the profile of the smoldering wave. In the RT mode, the gaseous combustion products move through the high-temperature area with a large amount of hot carbon. It leads to complete oxygen depletion as well as forming the zone of endothermic reactions, where carbon dioxide is reduced to monoxide.

On the other hand, Schult et al.² and Lempert et al.¹⁶ added that the RT mode can lead to quenching of combustion if the gas mass influx is large enough; incomplete conversion of carbon can occur because of cooling of the reaction by the fed gas at the inlet side of the reaction zone.

1.3. Potential Advantages and Drawbacks of the RT Mode in Oil Shale Applications. The RL mode for the combustion of oil shale has been studied extensively by Martins.¹⁷ In this mode and as illustrated in the top of Figure 1, most of the heat generated during smoldering combustion is left behind the combustion layer and is not used for oil displacement. Five reaction zones successively propagate in the combustion layer: drying zone, a zone of devolatilization, some time called distillation or cracking zone, the zone of low-temperature oxidation (LTO), the zone of FC oxidation also called high-temperature oxidation (HTO), and finally, the zone of CaCO₃ decarbonation following:



The zone of LTO is superposed with the zone of devolatilization. LTO corresponds to the partial direct oxidation of some oxygenated hydrocarbon. The oxygenated hydrocarbon compounds are formed when the oil molecules produced during devolatilization fix some unreacted oxygen coming from the FC zone.¹⁸ Generally, oxygen-consuming reactions that occur at temperatures lower than 350 °C are considered as LTO reactions. It has been shown that the LTO reactions increase the amount of fuel available as FC for combustion and cause a substantial decline in recoverable oil from the distillation and cracking zones.¹⁹ Thus, conditions that avoid LTO reactions must be maximized during the *in situ* combustion of heavy oils.¹⁹

In the RT mode (Figure 1b), the heat generated is blown downstream of the combustion layer. The high temperature of the heat-transfer layer is likely to cause a thermal cracking (devolatilization) of the fresh oil shale and to produce oil that will move ahead of the combustion layer, leaving a deposit of FC as fuel for the advancing combustion layer. Because all of the injected oxygen (in fed air) is likely to be consumed in the HTO zone in the combustion layer, it does not have the opportunity to react in LTO reactions with hydrocarbons elsewhere in the medium, especially in the heat-transfer layer. This is the main advantage of this mode.

Considering *in situ* oil recovery applications, the RT mode presents another advantage. Because the recovery process is essentially associated with the thermal front (cracking, eventual formation of an oil bank, etc.), as soon as the thermal front has crossed all of the zone to be exploited, the process can be stopped. The reaction front is far behind, and the FC will remain non-oxidized in a large zone. This would decrease the CO₂ emissions resulting from FC oxidation.

Another potential advantage of the RT propagation mode is its aptitude to cross large bands of inert material that the front may find during propagation. Indeed, the critical time for the extinction of a smoldering front is when the combustion layer enters inside an inert band. In the RL mode, the front will definitely extinguish if the inert band is thicker than the FC layer, which has been shown to be only several millimeters or centimeters thick.¹³ On the other hand, in the RT mode, when the combustion layer enters in the inert band, it stops consuming the fed oxygen, which will cross the hot zone downstream, and reignites the reactive layer just downstream of the inert band, if its temperature remains high enough.

Following this, a RT mode theoretically enables the front to cross inert layers as large as the high-temperature plateau, typically several meters thick. This mode of propagation is therefore promising for underground processing of media with heterogeneity between organic and inorganic material.

Theoretically speaking, the RT mode presents the advantage to offer a temperature control via the oxygen content in the fed air; this will be demonstrated in the Discussion about an Energy Balance Approach section at the end of the paper. This is one objective of this work to check experimentally this determining question. Indeed, if such a control is possible, one can expect to propagate "cold fronts" that do not decarbonate all CaCO₃ in the medium, which would result in lesser CO₂ emissions.

Nevertheless, the RT mode may present a drawback in terms of the required gas flow rate and the resulting pressure drop. In the RL mode, the front that pushes oil is the combustion layer, while it is the heat-transfer layer that pushes oil in the RT mode

(cf. Figure 1). The heat-transfer layer progresses at a quite small velocity, unless high gas flow rate is injected. As an example, to fix ideas, the velocity of the RL reaction front was about 4 mm min⁻¹ in a previous work, where air was fed at 0.021 m s⁻¹ in a medium containing 3.47% FC.¹⁴ In the RT mode, in the same medium and injection of a gas at 6.5% oxygen, the present work will show that it would be necessary to increase the gas velocity up to 0.056 m s⁻¹ for the heat-transfer layer to progress at the same velocity. Shifting from the RL mode to the RT mode would involve an increase of the pressure drop in the same ratio. This would imply an increase of the required pumping energy to feed the gas, which might be unacceptable.

This paper investigates the feasibility of the RT mode of smoldering combustion. The oil shales were originally chosen as the porous medium because of their energetic interest in oil recovery, as explained before. Experiments were carried out using oil shale semicoke for simplifying purposes, as detailed later. The impact of the oxygen content in the fed gas on smoldering characteristics, such as front temperature, propagation velocities of the different layers, and product gas release, is investigated.

Particular attention is paid to the fraction of CaCO₃ that is decarbonated at the front passage and the fraction of carbon that is oxidized to CO and not to CO₂.

2. EXPERIMENTAL SECTION

The same porous medium and sophisticated experimental device as described in refs 13 and 14 were used to operate smoldering.

2.1. Porous Medium. An oil shale porous medium, originating from the deposit of Timahdit in Morocco, is used in this work. The oil shale is first crushed and sieved to obtain sample sizes between 0.5 and 2 mm. Then, the oil shale is retorted at a temperature of 550 °C in a stainless-steel reactor externally heated by an electric rig furnace, under N₂ atmosphere and using a heating rate of 5 °C min⁻¹. The obtained oil shale semicoke was used for all experiments in this work. As explained into details in ref 14, the reasons for using semicoke (SC) instead of oil shale (OS) are that the SC does not lead to oil formation and transport, which is the case with OS. This makes it easy to establish a mass balance.

A horizontal tube furnace was used to characterize the initial OS, the prepared SC, and the solid residue after combustion. Details about the procedures can be found in ref 14.

The SC used in this work contains 6.95% FC; only 0.7% volatile matter remains instead of 14.7% in the initial OS.

2.2. Combustion Cell. Figure 2 presents the schematic diagram of the fixed-bed reactor used for our combustion tests.

Downward smoldering combustion tests were conducted in a vertical cylindrical combustion chamber of 91 mm inner diameter and a height of 300 mm, containing a mix of 50/50 mass % crushed oil shale semicoke and inert sand. This mix was indeed used as a reference porous medium in ref 14. The smoldering front is started at the top of the sample by a radiative heat flux of 50 kW m⁻² during 300 s, and the propagation is aided by a forced flow of air. A 1 cm layer of pure semicoke was put at the top of the bed to guarantee a good ignition. The temperature inside the reactor was measured by six thermocouples (T1, T2, T3, T10, T11, and T12) aligned along the axis of the reactor at different heights. The bed mass loss and pressure drop evolutions are recorded. Gas was sampled at the axis of the reactor near the bottom to quantify every 4 min CO and CO₂ by gas chromatography and O₂ using a paramagnetic analyzer in continuous mode.

After an experiment, the mass evolution of the system and gas composition values are interpreted on the basis of a mass balance for the smoldering front. Two values are derived from these data: the fraction of FC oxidized to CO, *fr*_{CO}, and the CaCO₃ decarbonated fraction, *fr*_{decarb}. Details about the procedure for the RL mode are given later in the paper.

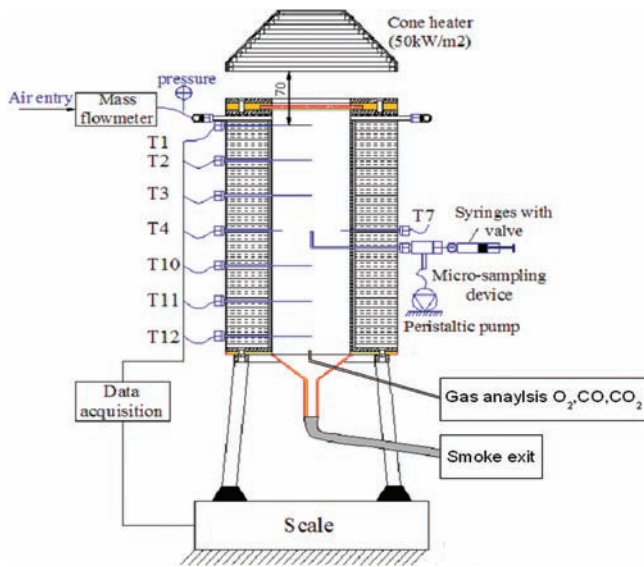


Figure 2. Cell combustion, with continuous gas sampling at the axis.

2.3. Present Investigation. The transition from RL to RT mode was obtained by decreasing the oxygen content in the fed air. This was obtained by mixing air with nitrogen. Experiments were conducted with a forced air flow of 0.085 m s^{-1} at standard temperature and pressure (STP). This flow rate is 4 times as high as previous experiments in the RL mode.¹⁴ This was adopted to increase the front velocity and to limit the duration of an experiment to around 1.5 h. This leads to classical front propagation velocities. Four molar fractions of oxygen were tested: 3.5, 4.5, 5.3, and 6.5%.

3. RESULTS AND DISCUSSION

Experiments with 6.5, 5.3, and 4.5% oxygen lead to a stable propagation of the combustion front. The experiment with 3.5% oxygen leads to front extinction. This was checked by repeating each experiment twice.

3.1. Temperature Profile. Figure 3 describes the evolution of the temperature within the column for an oxygen fraction of

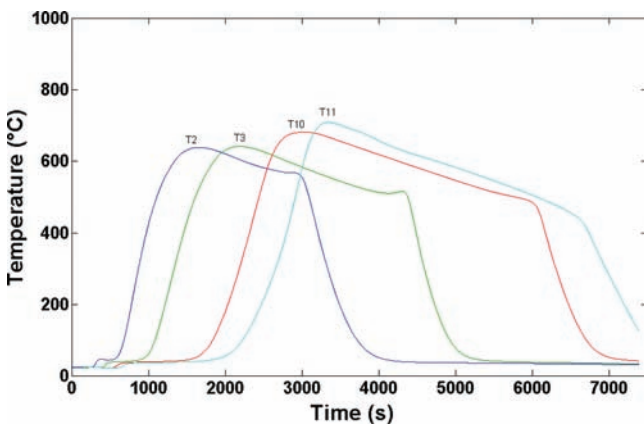


Figure 3. Typical time evolution of the temperature at several locations at the cell axis (T2, T3, T10, and T11). Experiment with $\text{O}_2 = 5.3 \text{ vol } \%$, and air superficial velocity = 0.085 m s^{-1} at STP.

5.3%, taken later as a representative example for all experiments. Each profile represents the temperature history at a specific location along the porous medium, as recorded by a thermocouple. Only thermocouples T2–T3–T10–T11 were selected. The temperature profile of thermocouples T1 and

T12 were removed because they correspond to the ignition region and the bottom of the reactor (where heat losses toward the environment are important), respectively.

For each temperature profile, two clear zones of increase and decrease of the temperature were observed. The zone of temperature increase corresponds to the passage of the heat-transfer layer, of which the velocity is faster than that of the combustion layer in the RT mode. The zone of the temperature decrease corresponds to the region where the fed air cools the medium after the reaction of FC oxidation has occurred. The heat-transfer layer and the zone of temperature decrease are separated by a zone of high but not constant temperature called semi-plateau. This zone is observed spreading out more and more during the smoldering propagation. This structure is characteristic of the RT mode, where a semi-plateau temperature appears between two regions corresponding to abrupt changes of the temperature. In previous work involving the RL mode,¹⁴ the semi-plateau was not clearly observed as in the present.

In RT mode experiments, a temperature peak was recorded. The reason for this is that the fed air flow rate is 4 times higher here than in previous experiments. Therefore, flattening of the plateau, which is due to heat losses, is attenuated here compared to the previous RL experiments, because of the higher air flow rate, leading to a higher advective heat flow rate.

The shape of a temperature profile inside the medium, at a given time, can be obtained qualitatively by inverting left and right the temperature history of a given thermocouple. Doing this with thermocouple T10 leads to Figure 4.

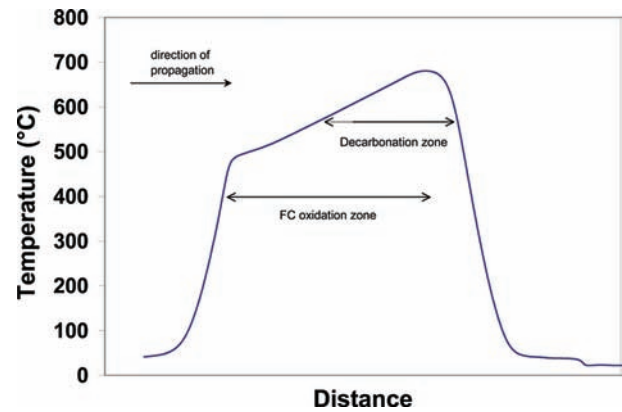


Figure 4. Possible localization of both zones of combustion and decarbonation in the temperature profile.

It can be seen in this figure that the temperature is higher in the heat-transfer layer (right) than in the following so-called chemical front (left). This is a surprising observation, if we refer to the theoretical discussion of ref 16, from which the higher temperature zone was expected to be located close to the combustion zone. The only explanation for this is that a significant part of an exothermic reaction is occurring in the heat-transfer layer. Because the only exothermic reaction known in the process is FC oxidation, this means that the FC oxidation zone is spread from the upstream of the temperature plateau, where it stops, to the heat-transfer layer downstream of the plateau. The explanation proposed is the following: it is thought that such an organization of the combustion layer and heat-transfer layer results from the fact that the oxygen content in the fed air is low and induces

globally low FC oxidation reaction rates and spreading of the FC oxidation zone. In the heat-transfer layer, the mass fraction of FC is higher than upstream and, despite the presence of the endothermic decarbonation of CaCO_3 , results in a high-medium temperature. Consequently, considering the result of TG tests of ref 20, indicating that FC oxidation is efficient starting from a temperature of $400\text{ }^\circ\text{C}$, FC oxidation is thought to expand in all of the zone at a temperature larger than approximately $400\text{ }^\circ\text{C}$. The FC oxidation (combustion zone) is also thought to stop around the temperature peak. This is a new vision of such fronts. It is illustrated in Figure 4 and will be discussed again later in the paper.

In the same figure, the location of the decarbonation reaction is indicated. It will be shown later that not all CaCO_3 is decarbonated at the passage of the front; therefore, this zone is thought to spread all over the medium at a temperature above $550\text{ }^\circ\text{C}$, for which decarbonation is efficient, as suggested by TG tests.¹⁴

The peak temperature obtained for all experiments is plotted in Figure 5 versus the oxygen content in the fed air. The

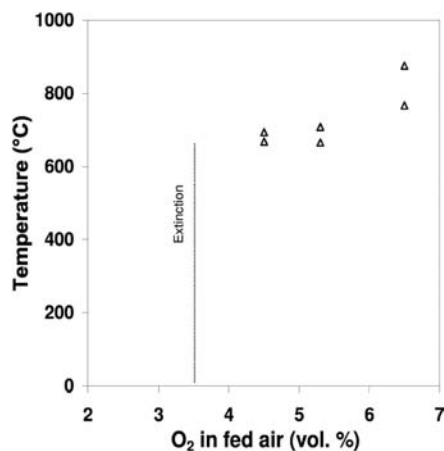


Figure 5. Peak temperature versus oxygen fraction in the fed air.

obtained temperatures are globally lower than the temperatures expected from an energy balance, as discussed in section 3.6. The heat losses throughout the walls are significant.

A clear increase of the temperature is observed as oxygen increases, to reach about $820\text{ }^\circ\text{C}$ at 6.5% oxygen. It is demonstrated here that, in the RT mode, the front temperature can be controlled by the amount of oxygen in the fed air. Globally, an increase of 1% oxygen leads to an increase of approximately $60\text{ }^\circ\text{C}$ in the peak temperature. An important result, for oil recovery applications, is that propagating *in situ* “cold fronts” is therefore possible in this mode. The RL mode does not offer this possibility because cold fronts are obtained by feeding gas with oxygen content larger than 21%, which is more expensive.

Extrapolating the temperature curve to the observed oxygen content leading to extinction, i.e., 3.5%, would lead to a value of about $600\text{ }^\circ\text{C}$. This value is similar to that of the coldest front that could be propagated in the RL mode by decreasing the content of FC in the medium, i.e., $580\text{ }^\circ\text{C}$.¹⁴ In all experiments, post-combustion analysis of the porous medium indicated that very few FCs were left after the passage of the front (0.25% in the residue). We show here that even cold fronts (*a priori* interesting to avoid CaCO_3 decarbonation) do not leave FC behind them. This indicates that quenching of the combustion

front never occurred in all experiments. It was observed in all carried out experiments that the propagation of the smoldering front consumes all supplied O_2 . The fact that all oxygen is consumed even at the temperature of $660\text{ }^\circ\text{C}$ (the coldest front in our experiments) is different from what was observed in the RL mode. From the results of ref 14, a front propagating at this temperature in the RL mode only uses approximately 30% of the fed oxygen and proportionally slows to the not used O_2 fraction. We believe that the reason why the cold front in the RT mode consumes more oxygen (rather than in the RL mode) is that oxygen crosses the large hot zone of the semi-plateau before leaving the front, resulting in a longer contact time with hot FC. This is not the case in the RL mode (cf. Figure 1).

3.2. Front Velocity. In the sequel of the paper, the heat-transfer layer, associated with the temperature increase, and the temperature decrease layer are by definition located where the temperature is equal to half of the temperature peak. With this definition, their position versus time is plotted in Figure 6 for

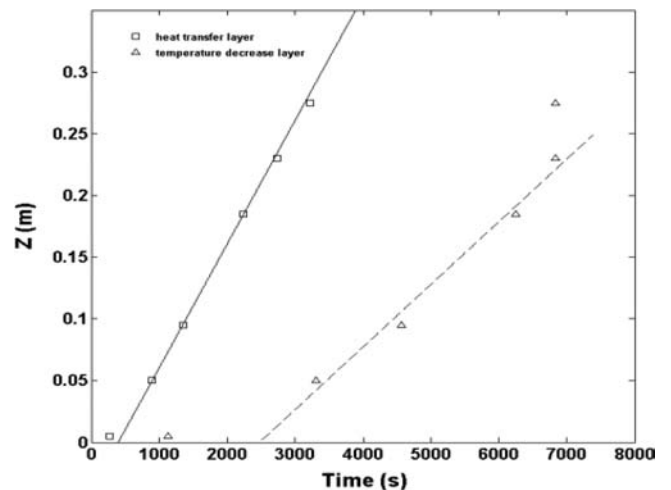


Figure 6. Position of the heat-transfer zone and the temperature decrease zone versus time.

the experiment with the oxygen fraction of 5.3%. If one excludes the points at the beginning of the column, where phenomena are established, and at the very end of the smoldering front propagation, a clear linear relation appears between the position of each layer and time.

The propagation velocities of the two layers, i.e., the curve slope, are constant but different. To our knowledge, observing clearly these two layers propagating regularly is a new and original result.

Figure 7 plots the velocities of the heat-transfer and temperature decrease layers obtained during all experiments with different oxygen fractions. The oxygen fraction for which extinction was observed is also indicated. The velocity of the temperature increase layer shows a clear increase with the O_2 fraction, while the heat-transfer layer velocity only increases slightly.

3.3. Produced Gases. Figure 8 shows the observed evolutions of O_2 , CO , and CO_2 mole fractions observed at the exit of the cell during the stable period of smoldering propagation. Globally, the values are shown to increase with the oxygen fraction in the fed air, which indicates that the smoldering combustion is in the oxygen-limited regime.²¹ As already mentioned in the paper, the oxygen is totally consumed

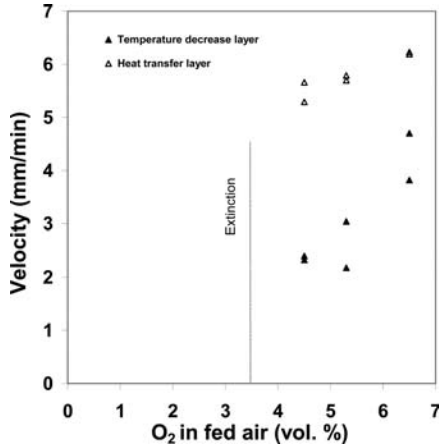


Figure 7. Velocities of the temperature decrease layer and the heat-transfer layer versus oxygen fraction in the fed air.

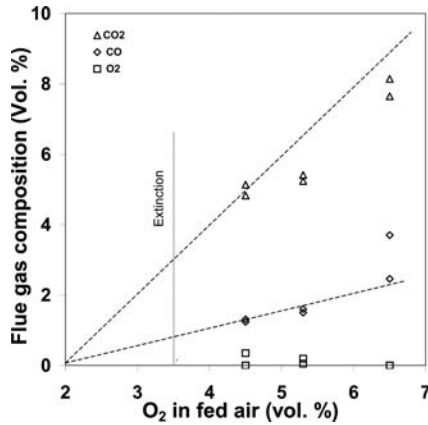
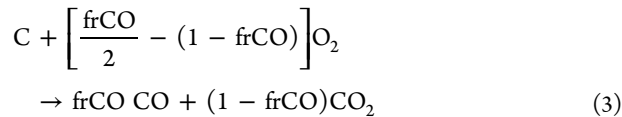


Figure 8. O₂, CO, and CO₂ concentrations in flue gas versus O₂ concentration in the fed air.

during all experiments; its fraction is equal to zero, up to measurement accuracy, in the exit gas regardless of the oxygen fraction in the fed air.

As discussed before, all of the FC was also consumed in all experiments carried out in this work. In this situation, the chemical front velocity is theoretically directly linked to three parameters: the amount of FC in the medium, the flow rate of oxygen fed to the front, and the fr_{CO} parameter that appears in the stoichiometric reaction.



This later parameter, fr_{CO} , is a consequence of the phenomena taking place in the porous medium.

The fractions of CO and CO₂ do not increase linearly with the oxygen fraction. CO was observed to increase in a faster way, and CO₂ was observed to increase in a less fast way; this indicates that the parameter fr_{CO} has probably increased in the experiments where oxygen was increased. This point will be discussed again later in this paper.

3.4. Identification of the Fraction of FC Oxidized to CO and the CaCO₃ Decarbonated Fraction. In a previous work related to experiments in the RL mode,¹⁴ it was shown that a parameter identification procedure, on the basis of a mass

balance for the combustion cell, can be used to determine the values of the fraction of carbon oxidized to CO, fr_{CO} , and the decarbonated fraction, fr_{decarb} . This was performed simultaneously with the identification of the two front (thermal and chemical) velocities, which were the same because of the presence of a single temperature peak, where the two fronts were grouped together.

In the present work involving the RT mode, a clear temperature semi-plateau appears. The first attempt to identify fr_{CO} and fr_{decarb} was based on the assumption that the thermal front corresponds to the temperature increase zone and the chemical front is located at the temperature decrease zone. The velocities of the temperature increase and temperature decrease zones were determined as explained before using the thermocouple signals. The thermal front velocity and the chemical front velocity were assimilated to them. Under this assumption, it is not possible to find a value for fr_{CO} and fr_{decarb} leading to a correct mass balance; large quantities of O₂ (several percentages) were always left in the flue gas according to the mass balance, when all O₂ is consumed in the experiments.

The second attempt was to try and identify both the thermal front velocity and the chemical front velocity together with fr_{CO} and fr_{decarb} . This approach was not successful; there are not enough data to identify four parameters, and nonphysical solutions were derived.

The third attempt was to consider that the thermal front was located at the temperature increase zone, thus, propagating at the same velocity, but that the velocity of the chemical front had to be identified. Doing this led to satisfactory mass balances, as reported below. It is interesting to note that the identified chemical front velocities were 1 mm min⁻¹ higher than the temperature decrease zone velocity but always smaller than the temperature increase zone velocity (or thermal front).

This confirms the point previously mentioned: the chemical front is probably not concentrated at the temperature decrease zone but probably spread toward the thermal front. The identified values for fr_{CO} and fr_{decarb} derived from the parameter identification procedure are plotted in Figure 9 versus the oxygen fraction in the fed air. The results are commented below. The fr_{CO} parameter increases regularly with oxygen fraction from 0.29 at 4.5% O₂, where the front temperature was about 660 °C, to 0.43 at 6.5% O₂, where the front temperature was about 820 °C. This confirms quantitatively the previous indication (see Figure 8) of the

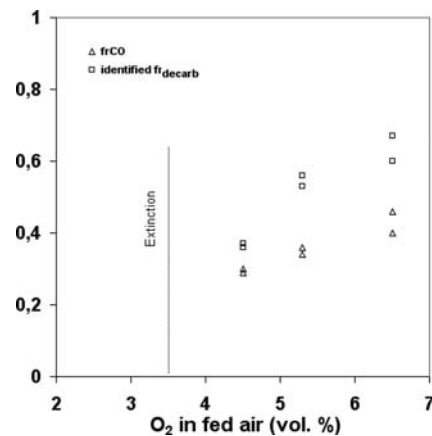


Figure 9. Identified values for the fraction of carbon oxidized to CO and the fraction of CaCO₃ decarbonated.

increase of frCO . The same tendency of the frCO increase with the front temperature increase was observed in previous work in the RL mode. The range of values is slightly higher in the RT mode (0.29–0.43) than in the RL mode (0.19–0.35).

Figure 9 also gives the identified decarbonated fraction of CaCO_3 as a function of the oxygen fraction. A decrease of the decarbonated fraction was observed from 63 to 37% by decreasing the oxygen fraction in the fed air. This result is very important and represents one of the main objectives of this work. Indeed, it is possible to propagate a smoldering front in the RT mode at 660°C by feeding it with 4.5% oxygen, and only 37% of the present CaCO_3 will be decarbonated at the passage of the front.

3.5. Localization of the FC Oxidation and the CaCO_3 Decarbonation Zones. The question of an eventual spreading of the FC oxidation zone has been raised in this paper. The same question is asked concerning the CaCO_3 decarbonation zone location and its thickness. A new and original gas microsampling system with online gas analysis was set up and experimented.

The idea is to follow the variation of the fractions of O_2 and CO_2 in the gas phase before, during, and after the passage of the smoldering front. The thickness and localization of the FC oxidation and the CaCO_3 decarbonation zones were determined consequently.

The gas were sucked at the center of the reactor through a 1.6 mm internal diameter tube. A paramagnetic analyzer was used to analyze the oxygen, and a nondispersive infrared (NDIR) analyzer was used to analyze the carbon dioxide. The sampled flow rate was fixed at 0.60 L min^{-1} at STP, corresponding approximately to 55 times less than the flow rate fed to the combustion cell (33.2 L min^{-1} at STP), to minimize the perturbation of the front. To obtain this, the analyzers sucked 1.60 L min^{-1} at STP, which consisted of 1 L min^{-1} at STP of N_2 fed from a mass flow meter/controller and 0.60 L min^{-1} at STP sampled in the cell. Therefore, the measured O_2 and CO_2 fractions were divided by 2.67 compared to that in the sampled gas. The CO fraction was not reported here because it saturated the NDIR analyzer.

Figure 10 plots the time evolution of the oxygen and carbon dioxide fractions versus time for the experiment with 5.3% O_2 . For better interpretation of the results, the oxygen and carbon dioxide fractions were time-derived and also plotted in Figure 10. Finally, for indication, a reconstituted temperature at the sampling point was added. Because there is no thermocouple at the microsampling point situated at the center of the cell, the plotted temperature is an average between the upstream temperature (T3) and downstream temperature (T10) of the sampling points.

At the beginning of the experiment, the front is upstream of the sampling point. The oxygen fraction close to zero confirms that oxygen was used during the smoldering front propagation. An unstable value of the carbon dioxide fraction was observed near 1.5%.

Two zones of CO_2 decrease were then observed: (i) the first zone, between 1780 and 3515 s, in which a rapid decrease of the CO_2 fraction from 1.5 to 0.74% was observed (this decrease can be attributed to the passage of the CaCO_3 decarbonation zone, where CO_2 was produced), and (ii) a second zone, between 3725 and 5600 s, where the CO_2 fraction decreases more slowly from 0.74 to 0% (in this zone, the oxygen fraction increased proportionally to the decrease of CO_2 , which

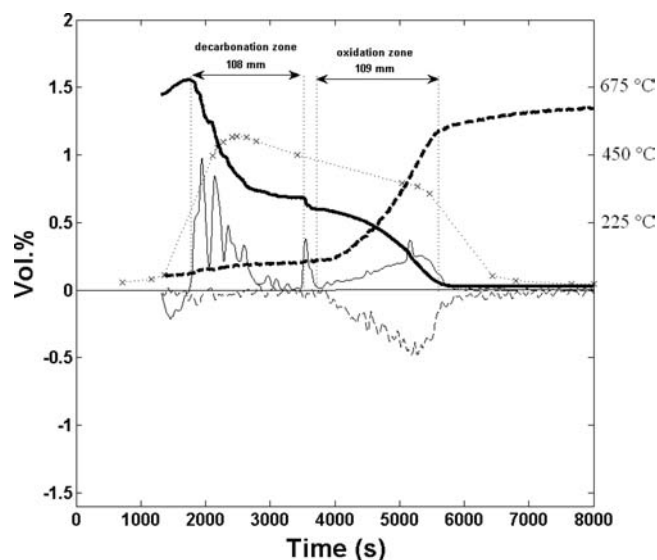


Figure 10. Time evolution of the fractions of oxygen (bold dotted line) and carbon dioxide (bold solid line), derivative curves of oxygen (dotted line) and carbon dioxide (solid line) signals, and temperature profile (cross symbols).

indicates that this zone corresponds to the main FC oxidation zone).

Afterward, both decarbonation and FC oxidation zone thicknesses were estimated using the transition time and the considered layer velocity, as determined before. Both the decarbonation zone and the FC oxidation zone have a thickness of about 110 mm. This confirms the fact that both zones are displayed in the space.

In the so-called decarbonation zone, a slight evolution of the O_2 fraction can be observed. This indicates that some oxidation of carbon occurs in this zone. This combustion may explain the fact that the peak temperature is located in the endothermic decarbonation zone, as discussed in the Temperature Profile section of the paper.

A remarkable thin zone of abrupt CO_2 decrease was observed between 3515 and 3725 s. The phenomenon was observed again when repeating the experiment. In this time period, only a slight oxygen fraction increase is observed. Therefore, it is not thought that any oxidation (of FC or gaseous CO) is at the origin of this peak. The proposed explanation is that the decarbonation reaction may abruptly change rate because the parameters that control the reaction kinetics vary significantly around this zone. These parameters are the temperature and partial pressure of CO_2 .

They both have a nonlinear impact on the reaction kinetics referring to the works of refs 21 and 22. The changes in these parameters may also be responsible for the peaks in the time derivative curve for the CO_2 fraction in the decarbonation zone. No clear conclusion can nevertheless be formulated at this stage.

The obtained O_2 fraction evolution can also be used to discuss the probability for LTO to occur in the case of smoldering in oil shales. In the RT mode, as discussed before and illustrated in Figure 1, LTO reactions may occur near the devolatilization zone, which corresponds here to the temperature increase zone located at short times in Figure 10. We show here that, in this zone, the amount of O_2 is very small, less than 0.6% (in the nondiluted sample). This is likely to minimize the progress of LTO reactions.

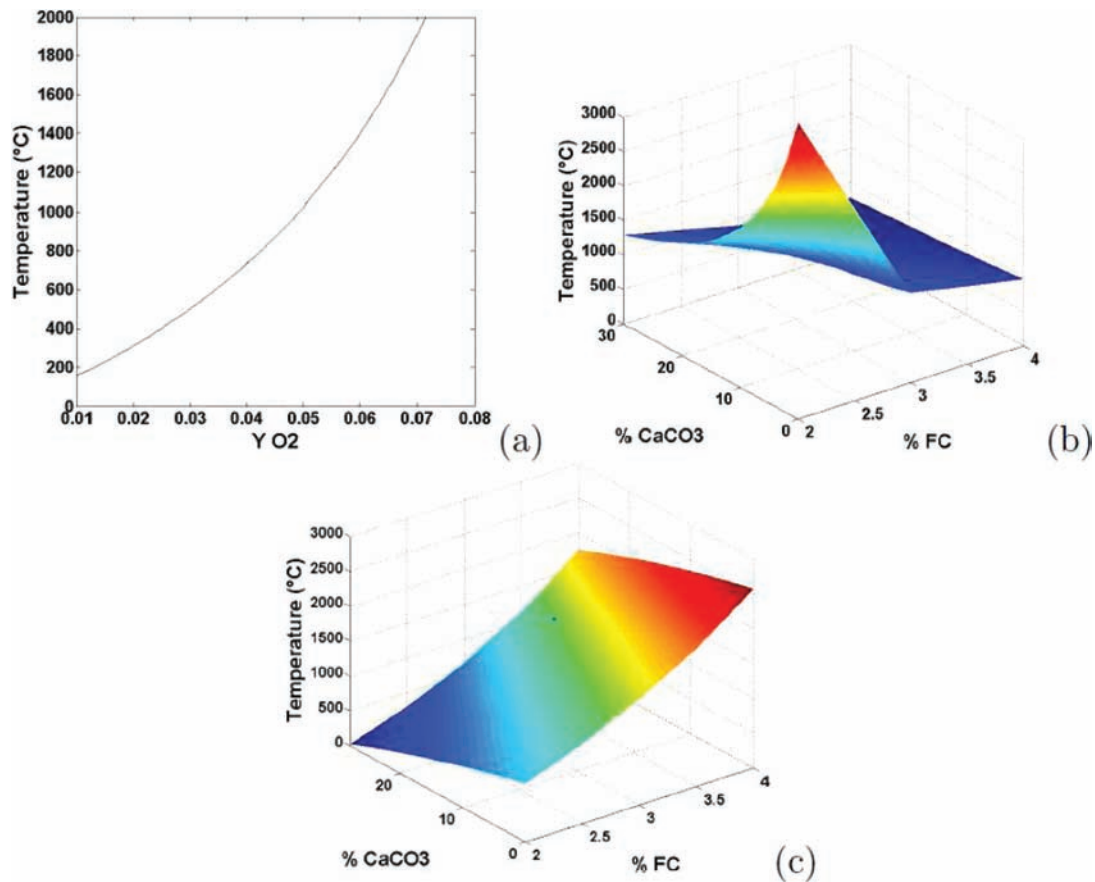


Figure 11. Theoretical temperature of the front in the RT mode versus (a) the molar fraction of oxygen in the fed air, and (b) the medium composition in FC and CaCO₃ of the porous medium. (c) Results in RL mode are reminded. The reference conditions for all cases are 3.5% FC, 22.4% CaCO₃, and 4.5% O₂ in the fed air.

3.6. Discussion about an Energy Balance Approach. In a previous paper,¹⁴ we have shown that establishing an energy balance for the two propagation layers in the RL mode enabled us to calculate a theoretical plateau temperature. Confronting the theoretical values to experimental values obtained for a large range of porous medium composition in terms of FC content and CaCO₃ content indicated that this approach was not accurate but followed the trends observed experimentally. The difference between a calculated plateau temperature and an experimental value was typically 250 °C. The energy balance approach is applied here to the RT mode as detailed below and brings several interesting indications. Details of the equations used to calculate the plateau temperature from an energy balance in the RT mode are reported in the Appendix.

We have plotted in Figure 11a the theoretical evolution of the plateau temperature versus the fraction of oxygen in the fed air for a medium containing 3.47% FC and 22.4% CaCO₃ as the one used in experiments. This graph confirms that oxygen content is theoretically a parameter controlling the front temperature, and this motivated the present work. It is also particularly interesting for *in situ* applications; the temperature of the front can theoretically be controlled via this parameter, with oxygen contents smaller than that in air. Note that, in the RL mode, this parameter cannot be used practically to lower the front temperature because this would require the use of oxygen-enriched air.

In Figure 11b, we have plotted the plateau temperature versus two parameters that characterize the porous medium in

which the front is propagated: the FC content, whose oxidation supports the chemical front progress, and the amount of CaCO₃ that is decarbonated at the passage of the front, which acts as a heat sink. In the case of the RL mode, the composition of the medium can strongly impact the plateau temperature (Figure 11c); this was checked experimentally in ref 14. In the case of the RT mode, the energy balance indicates that the plateau temperature is poorly influenced by the composition of media containing more than 3% FC. This may have important consequences for *in situ* applications; it tends to demonstrate that a RT smoldering front could be more robust than a RL smoldering front, because the RT front plateau temperature will not change as the composition of the porous medium changes from one location to another in the field. This nevertheless remains to be demonstrated experimentally.

Finally, the theoretical plateau temperature corresponding to each case experimented in this work was calculated and compared to experimental values. It was found that the experimental values are much smaller than the calculated values. Differences were typically 1500 °C, much larger than in the previous study of the RL mode.¹⁴ The explanation proposed here is that, for experiments in the RT mode, the FC oxidation zone spreads over a large zone and results in very important heat losses and a temperature decrease. In the case of the RL mode, this problem was avoided because the FC oxidation was concentrated at a thin temperature peak and induced much less heat losses. At this stage, further

experimental investigations are required to validate this explanation.

4. CONCLUSION

The main goal of this work was to investigate the feasibility of propagating a smoldering front in the RT mode in oil shale or semicoke porous media. We showed that it is possible to propagate the smoldering front with different oxygen fractions in a stable and repeatable way. A low limit value of the oxygen fraction has been identified at 3.5%, leading to extinction. The observed temperature profiles and velocities correspond qualitatively to those theoretically characterizing the RT mode. We showed that the front temperature can be controlled by the oxygen content in the fed gas; an increase of 1% of oxygen leads to an increase of approximately 60 °C in the peak temperature.

The smoldering velocity is also a consequence of oxygen availability. The combustion layer velocity increases from 2.4 to 4.26 mm min⁻¹ by increasing the oxygen fraction from 4.5 to 6.5%.

Thanks to the microsampling and analysis device, the combustion layer is shown not to be concentrated at the upstream of the plateau but to spread over a large zone of 110 mm. This RT mode leads to strongly limit the *in situ* decarbonation. Decarbonated fractions as low as 80 and 44% are obtained with oxygen fractions from 6.5 to 4.5%, respectively, when, in the RL mode, full decarbonation was observed. The decarbonation zone is also shown to spread over a large zone. Even in the case of the coldest front at 660 °C, all of the fed oxygen is consumed, contrary to the case of the RL mode. All of the FC in the medium was found to oxidize. The fraction of FC oxidized into CO was evaluated between 0.29 and 0.43. This percentage increases with the temperature, as in the case of the RL mode.

We also showed that LTO reactions should be minimized in the case of smoldering in oil shales because only very few oxygen compounds are present in the zone where devolatilization occurs.

■ APPENDIX

Calculation of the plateau temperature from an energy balance over a smoldering front, for the case of the RT mode ($\delta > 1$).

A representation of a smoldering front in the RT mode ($\delta > 1$) is given in Figure 12. A general case is considered here, in which the virgin medium called fuel will form smoke during combustion of FC and CO₂ because of decarbonation of the mineral matrix. The decarbonation reaction is assumed to occur at the heat-transfer layer. The combustion layer travels at a velocity lower than the heat-transfer layer velocity. Therefore

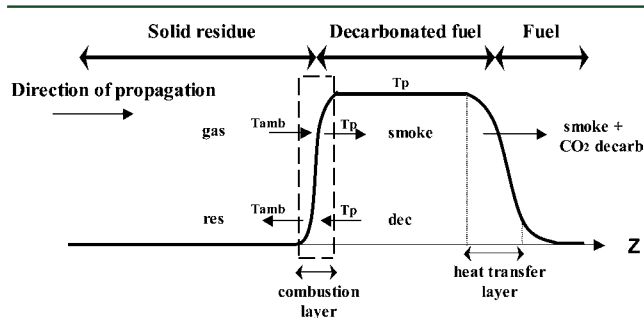


Figure 12. RT front structure.

$$\delta = \frac{v_{\text{frt}}}{v_{\text{frc}}} > 1 \quad (4)$$

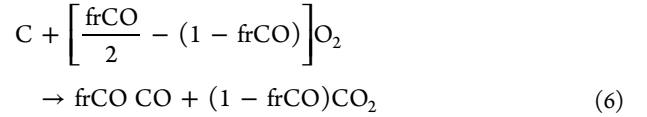
Combustion Layer Velocity, v_{frc}

The velocity of the combustion layer can be calculated from a balance on O₂ species, expressing that the molar flux density consumed by the reaction equals the molar flux transported by air.²⁰

The molar flux density of FC oxidized by the combustion layer is (in mol s⁻¹ m⁻²)

$$\frac{v_{\text{frc}} \rho_{\text{fu}} x_{\text{FC}} \text{fr}_{\text{oxi}}}{M_{\text{C}}} \quad (5)$$

The FC oxidation to CO and CO₂ is written



Therefore, the oxidation of 1 mol of C requires $(1 - \text{frCO}/2)$ mol of O₂, and the molar flux density of O₂ required by the combustion layer can be expressed as (in mol s⁻¹ m⁻²)

$$\frac{v_{\text{frc}} \rho_{\text{fu}} x_{\text{FC}} \text{fr}_{\text{oxi}}}{M_{\text{C}}} \left(1 - \frac{\text{frCO}}{2} \right) \quad (7)$$

The molar flux density of air fed to the combustion layer is

$$\frac{v_{\text{g}} \rho_{\text{g}}}{M_{\text{g}}} \quad (8)$$

and, using the molar fraction of O₂ in the air y_{O_2} , the molar flux density of O₂ fed to the combustion layer is

$$\frac{v_{\text{g}} \rho_{\text{g}}}{M_{\text{g}}} y_{\text{O}_2} \quad (9)$$

Equating eqs 7 and 9, we have

$$v_{\text{frc}} = \frac{v_{\text{g}} \rho_{\text{g}}}{M_{\text{g}}} y_{\text{O}_2} \frac{M_{\text{C}}}{\rho_{\text{fu}} x_{\text{FC}} \text{fr}_{\text{oxi}} \left(1 - \frac{\text{frCO}}{2} \right)} \quad (10)$$

Heat-Transfer Layer Velocity, v_{frt}

A thermal balance over the heat-transfer layer can be written as

$$\begin{aligned} \dot{m}_{\text{sm}} C_{\text{p}_{\text{sm}}} (T_{\text{p}} - T_{\text{ref}}) + \dot{m}_{\text{fu}} C_{\text{p}_{\text{fu}}} (T_{\text{amb}} - T_{\text{ref}}) - \dot{m}_{\text{dec}} \\ C_{\text{p}_{\text{dec}}} (T_{\text{p}} - T_{\text{ref}}) - \dot{m}_{\text{sm}} C_{\text{p}_{\text{sm}}} (T_{\text{amb}} - T_{\text{ref}}) - \dot{m}_{\text{CO}_2} \\ C_{\text{p}_{\text{CO}_2}} (T_{\text{amb}} - T_{\text{ref}}) - \dot{m}_{\text{CaCO}_3} \Delta H_{\text{CaCO}_3} \\ = 0 \end{aligned} \quad (11)$$

where T_{ref} is a reference temperature. The calorific value for SC and solid residue was fixed at 830 J kg⁻¹ K⁻¹.

Taking T_{amb} as the reference temperature leads to

$$\begin{aligned} \dot{m}_{\text{sm}} C_{\text{p}_{\text{sm}}} (T_{\text{p}} - T_{\text{amb}}) - \dot{m}_{\text{dec}} C_{\text{p}_{\text{dec}}} (T_{\text{p}} - T_{\text{ref}}) - \dot{m}_{\text{CaCO}_3} \Delta \\ H_{\text{CaCO}_3} = 0 \end{aligned} \quad (12)$$

where

$$\dot{m}_{\text{CaCO}_3} = v_{\text{frt}} \rho_{\text{fu}} x_{\text{CaCO}_3} \text{fr}_{\text{decarb}}$$

$$\dot{m}_{\text{dec}} = v_{\text{frt}} \rho_{\text{fu}} \text{fr}_{\text{decarb}}$$

$$\text{fr}_{\text{dec}} = \left[x_{\text{CaCO}_3}(1 - \text{fr}_{\text{decarb}}) + x_{\text{CaCO}_3} \text{fr}_{\text{decarb}} \frac{M_{\text{CaO}}}{M_{\text{CaCO}_3}} + x_{\text{FC}} + x_{\text{in}} \right]$$

and

$$\dot{m}_{\text{sm}} = \rho_g v_g$$

$$C_{p_{\text{sm}}} = C_{p_g}$$

Then, we may write

$$v_{\text{fr}} = \frac{\dot{m}_{\text{sm}} C_{p_{\text{sm}}} (T_p - T_{\text{amb}})}{\rho_{\text{fu}} \text{fr}_{\text{decarb}} C_{p_{\text{dec}}} (T_p - T_{\text{amb}}) + \rho_{\text{fu}} x_{\text{CaCO}_3} \text{fr}_{\text{decarb}} \Delta H_{\text{CaCO}_3}} \quad (13)$$

Plateau Temperature

The thermal balance over the combustion layer can be written as

$$\begin{aligned} \dot{m}_g C_{p_g} (T_{\text{amb}} - T_{\text{ref}}) + \dot{m}_{\text{dec}} C_{p_{\text{dec}}} (T_p - T_{\text{ref}}) + \dot{m}_{\text{FC}} \Delta H_{\text{FC}} \\ - \dot{m}_{\text{res}} C_{p_{\text{res}}} (T_{\text{amb}} - T_{\text{ref}}) - \dot{m}_{\text{sm}} C_{p_{\text{sm}}} (T_p - T_{\text{ref}}) \\ = 0 \end{aligned} \quad (14)$$

Taking T_p as the reference temperature leads to

$$\dot{m}_g C_{p_g} (T_{\text{amb}} - T_p) + \dot{m}_{\text{FC}} \Delta H_{\text{FC}} - \dot{m}_{\text{res}} C_{p_{\text{res}}} (T_p - T_{\text{ref}}) = 0 \quad (15)$$

or

$$T_p = \frac{\dot{m}_{\text{FC}} \Delta H_{\text{FC}}}{\dot{m}_g C_{p_g} - \dot{m}_{\text{res}} C_{p_{\text{res}}}} + T_{\text{amb}} \quad (16)$$

where

$$\dot{m}_{\text{FC}} = v_{\text{fr}} \rho_{\text{fu}} x_{\text{FC}}$$

$$\dot{m}_g = (v_g - v_{\text{fr}}) \rho_g$$

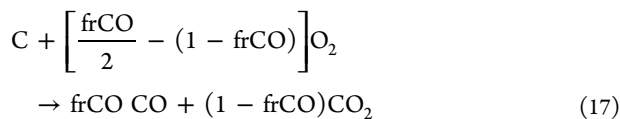
because we have $v_{\text{fr}} \ll v_g$, then $\dot{m}_g = v_g \rho_g$

$$\dot{m}_{\text{res}} = v_{\text{fr}} \rho_{\text{fu}} \text{fr}_{\text{res}}$$

$$\text{fr}_{\text{res}} = \left[x_{\text{CaCO}_3}(1 - \text{fr}_{\text{decarb}}) + x_{\text{CaCO}_3} \text{fr}_{\text{decarb}} \frac{M_{\text{CaO}}}{M_{\text{CaCO}_3}} + x_{\text{in}} \right]$$

Heat of reactions:

The FC oxidation reaction may be written as



According to Hess's law, we have (with our sign definition)

$$\Delta H_{\text{FC}} = 110.5 \text{frCO} + 396.5(1 - \text{frCO}) \quad \text{kJ mol}^{-1}$$

The decarbonation reaction may be written as



According to Hess's law, we have (with our sign definition)

$$\begin{aligned} \Delta H_{\text{CaCO}_3} &= -635.1 - 393.5 + 1207 = +178.4 \\ &\text{kJ mol}^{-1} \text{CaCO}_3 \end{aligned}$$

AUTHOR INFORMATION

Corresponding Author

*E-mail: mohamed.sennoune@mines-albi.fr.

Notes

The authors declare no competing financial interest.

ACKNOWLEDGMENTS

The authors are most grateful to Bernard Auduc for his technical support during all experiments.

NOMENCLATURE

Components

C = carbon

CaCO₃ = calcium carbonate

FC = fixed carbon

in = inert

Greek Symbols

δ = ratio between thermal and chemical front velocities

ρ = volumetric mass (kg m⁻³)

Others

fr_c = chemical front

fr_t = thermal front

Physical Symbols

\dot{m} = mass flow rate in the front frame (kg s⁻¹)

ΔH = reaction heat (J mol⁻¹)

C_p = calorific capacity (J kg⁻¹ K⁻¹)

fr = fraction

frCO = fraction of FC oxidized into CO

M = molar mass (g mol⁻¹)

p = plateau

T = temperature (°C)

v = velocity (m s⁻¹)

y = molar fraction

Reactions

decarb = decarbonated

oxi = oxidized carbon

Subscript Materials

fu = fuel

g = gas

res = solid residue

sm = smoke

dec = decarbonated fuel

REFERENCES

- (1) Rein, G. Smouldering combustion phenomena in science and technology. *Int. Rev. Chem. Eng.* **2009**, *1* (1), 3–18.
- (2) Schult, D.; Matkowsky, B.; Volpert, V.; Fernandez-Pello, A. Forced forward smolder combustion. *Combust. Flame* **1996**, *104* (1–2), 1–26.
- (3) Aldushin, A.; Rumanov, I.; Matkowsky, B. Maximal energy accumulation in a superadiabatic filtration combustion wave. *Combust. Flame* **1999**, *118* (1–2), 76–90.
- (4) Elayeb, M. Modélisation à l'échelle microscopique de transports avec réaction en milieu poreux: Combustion en lit fixe. Ph.D. Thesis, Université de Poitiers, Poitiers, France, 2008.
- (5) Egerton, A.; Guban, K.; Weinberg, F. The mechanism of smouldering in cigarettes. *Combust. Flame* **1963**, *7*, 63–78.

- (6) Torero, J.; Fernandez-Pello, A. Forward smolder of polyurethane foam in a forced air flow. *Combust. Flame* **1996**, *106* (1–2), 89–109.
- (7) Carvalho, E. R.; Gurgel Veras, C. A.; Carvalho, J. A., Jr. Experimental investigation of smouldering in biomass. *Biomass Bioenergy* **2002**, *22* (4), 283–294.
- (8) Vantelon, J.; Lodeho, B.; Pignoux, S.; Ellzey, J.; Torero, J. Experimental observations on the thermal degradation of a porous bed of tires. *Proc. Combust. Inst.* **2005**, *30* (2), 2239–2246.
- (9) Zhou, H.; Jensen, A.; Glarborg, P.; Jensen, P.; Kavaliauskas, A. Numerical modeling of straw combustion in a fixed bed. *Fuel* **2005**, *84* (4), 389–403.
- (10) Ryu, C.; Phan, A.; Yang, Y.; Sharifi, V.; Swithenbank, J. Ignition and burning rates of segregated waste combustion in packed beds. *Waste Manage.* **2007**, *27* (6), 802–810.
- (11) Pironi, P.; Switzer, C.; Rein, G.; Fuentes, A.; Gerhard, J.; Torero, J. Small-scale forward smouldering experiments for remediation of coal tar in inert media. *Proc. Combust. Inst.* **2009**, *32* (2), 1957–1964.
- (12) Rein, G.; Cohen, S.; Simeoni, A. Carbon emissions from smouldering peat in shallow and strong fronts. *Proc. Combust. Inst.* **2009**, *32* (2), 2489–2496.
- (13) Martins, M.; Salvador, S.; Thovert, J.; Debenest, G. Co-current combustion of oil shale—Part 2: Structure of the combustion front. *Fuel* **2010**, *89* (1), 133–143.
- (14) Sennoune, M.; Salvador, S.; Quintard, M. Reducing CO₂ emissions from oil shale semicoke smoldering combustion by varying the carbonate and fixed carbon contents. *Combust. Flame* **2011**, *158* (11), 2272–2282.
- (15) Voice, E.; Wild, R. Importance of heat transfer and combustion in sintering. *Iron Coal Trades Rev.* **1957**, *175*, 841–850.
- (16) Lempert, D.; Glazov, S.; Manelis, G. Mass transfer in filtration combustion processes. In *Mass Transfer in Multiphase Systems and Its Applications*; El-Amin, M., Ed.; InTech: Rijeka, Croatia, 2011; Chapter 21, pp 483–498.
- (17) Martins, F. The structure of a combustion front propagating in a fixed bed of crushed oil shale: Co-current configuration. Ph.D. Thesis, Université de Toulouse, Toulouse, France, 2008.
- (18) Sarathi, P. *In-Situ Combustion Handbook—Principles and Practices*, Technical Report; National Petroleum Technology Office: Tulsa, OK, 1999; DOE/PC/91008-0374.
- (19) Martins, M.; Salvador, S.; Thovert, J.; Debenest, G. Co-current combustion of oil shale—Part 1: Characterization of the solid and gaseous products. *Fuel* **2010**, *89* (1), 144–151.
- (20) Ohlemiller, T. Modeling of smoldering combustion propagation. *Prog. Energy Combust. Sci.* **1985**, *11* (4), 277–310.
- (21) Rao, T.; Gunn, D.; Bowen, J. Kinetics of calcium carbonate decomposition. *Chem. Eng. Res. Des.* **1989**, *67* (1), 38–47.
- (22) Garcia-Labiano, F.; Abad, A.; De Diego, L.; Gayán, P.; Adánez, J. Calcination of calcium-based sorbents at pressure in a broad range of CO₂ concentrations. *Chem. Eng. Sci.* **2002**, *57* (13), 2381–2393.